



Contents lists available at ScienceDirect

# Journal of Molecular Catalysis A: Chemical

journal homepage: [www.elsevier.com/locate/molcata](http://www.elsevier.com/locate/molcata)



## Nanostructured MFI-type zeolites as catalysts in glycerol etherification with *tert*-butyl alcohol

Nathália Simone<sup>a,b</sup>, Wagner A. Carvalho<sup>a,\*</sup>, Dalmo Mandelli<sup>a</sup>, Ryong Ryoo<sup>b</sup>

<sup>a</sup> Centro de Ciências Naturais e Humanas, Universidade Federal do ABC, Rua Santa Adélia, 166, Santo André—SP CEP 09210-170, Brazil

<sup>b</sup> Center for Functional Nanomaterials, Department of Chemistry, and Graduate School of Nanoscience and Technology (WCU), KAIST, Daejeon 305-701, Republic of Korea

### ARTICLE INFO

#### Article history:

Received 28 September 2015

Received in revised form 1 February 2016

Accepted 2 February 2016

Available online xxx

#### Keywords:

Hierarchical zeolite

Mesoporous material

Surfactant-directed synthesis

Glycerol etherification

### ABSTRACT

Hierarchical zeolite possessing MFI framework type was hydrothermally prepared using  $C_{22}H_{45}-N^+(CH_3)_2-C_6H_{12}-N^+(CH_3)_2-C_6H_{13}$  as a structure-directing agent in a seed-assisted synthesis method. The nanospunge-like morphology was composed of a three-dimensional disordered network of MFI layers with 2.5 nm thickness supporting each other. Catalytic performance of the MFI nanospunge was investigated in glycerol etherification with *tert*-butyl alcohol in liquid phase and compared to conventional microporous MFI zeolite and MFI unilamellar nanosheet. The hierarchical zeolites were much more active, which can be attributed to the acid sites located on the external surfaces accessible for the reaction of bulky reactants.

© 2016 Elsevier B.V. All rights reserved.

### 1. Introduction

Crystalline aluminosilicates possessing a system of mesopores in addition to their intrinsic microporous architecture are called hierarchical zeolites, and are an emerging new area in the mature field of zeolites. Despite the remarkable features of the microporous structure, the dimensionality and narrowness of the conventional porous system of zeolites often severely limit the surface accessibility and diffusion of bulky species. Reactants and products with sizes beyond the micropore dimensions cannot diffuse into and out of zeolite crystals, and compromise their diffusion, even in the case of smaller molecules, limiting the catalytic performance. Bulk zeolite crystals are often several thousand times larger than the pore diameter, and in such a system, less than 10% of zeolite active sites at the edge of the bulky crystal might actually participate in the catalytic reaction simply due to the limited mass transport to and from these active sites [1]. In addition, slow diffusion can cause polymerization of by-products or reaction intermediates covering catalytic active sites within the microporous channels. As heterogeneous acid catalysts, hierarchical zeolites have been gathering increasing attention for their potential to resolve diffusion and mass transfer limitations of microporous zeolites, and owing to a high concentration of external acid sites in the structure of the solids. Moreover,

these acid sites have been proven to be stronger than those of mesoporous materials such as MCM-41 [2]. More recently, hierarchical zeolites have demonstrated an attractive catalytic performance in a number of bulky molecular reactions requiring strong acid sites, thereby presenting a promising alternative to their bulk counterpart for a wide range of catalytic applications [3–5].

Over the years, exploratory work has led to the synthesis of hierarchical zeolites using top-down or bottom-up approaches. Of the top-down strategies, post-synthetic demetallation [6–9] and delamination [10,11] have been amongst the most commonly reported. In particular, demetallation has found practical application at a mass-production scale, and its applicability depends heavily on structures of the zeolite framework and Si/Al ratios. Unfortunately, depending on the selected conditions, framework defect sites are often generated, leading to a decrease in crystallinity and a poor hydrothermal or thermal stability when compared to the bulk analogue. Usually, mesopore diameters obtained in this manner are not uniform. Instead, zeolite synthesis methods using templates are suitable for generating uniform mesopores.

Bottom-up strategies involve a modification of the synthesis protocol, wherein multiammonium surfactants [6,12–14], hard templates [15] or organosilane surfactants [16,17] are employed as mesopore structure-directing agents (SDAs). Employing these templates, zeolite crystals can be grown within a limited space confined by the template pore walls. The templates can be removed after the zeolite crystallization through a combustion process. As these

\* Corresponding author. Fax: +55 1149968386.

E-mail address: [wagner.carvalho@ufabc.edu.br](mailto:wagner.carvalho@ufabc.edu.br) (W.A. Carvalho).

approaches often involve substantial amounts of costly templates, the newly formulated solid must provide a clear economic benefit that justifies the added investment cost. Choi et al. [12] introduced an effective strategy to synthesize extremely thin nanosheets of MFI type zeolite by using multiammonium surfactants to form a crystalline MFI structure, while self-assembled long hydrophobic chains direct the crystal morphology into a lamellar mesostructure. The fact that no other conventional SDA, as tetrapropylammonium, was required confirms that a zeolitic microporous architecture can be simply synthesized using the porogenic activity of a functional group of the template molecule. Thus, depending on the synthesis conditions, it is possible to synthesize MFI zeolite nanosheets as either a fully disordered assembly, or through regular stacking into an ordered multilamellar mesostructure. The synthesis of hierarchical MFI zeolite was later performed by adding small amounts of bulk MFI zeolite seeds [14]. Seeding was confirmed to dramatically reduce the zeolite crystallization time and surprisingly resulted in the formation of a nanospunge like morphology. The mesopore diameters in this case could also be systematically tailored by varying the length of the alkyl tails, with the resulting MFI zeolite nanosheets exhibiting a remarkably high mechanical strength, a thermal and hydrothermal stability comparable to the bulk counterpart and a strong Brønsted acidity at the external surface [14]. Enhanced catalytic performances were witnessed in different catalytic applications owing to a large number of active sites on the external surface of the nanosheets and the short diffusion pathways inside the crystal framework [6].

In recent years, the processing of a glycerol is gaining attention due to its increasingly surplus from the biodiesel production. With more than 1500 known end uses, it is produced during biodiesel manufacture, by transesterification of vegetable oils with methanol, as by-product, accounting for 10 wt% of the total product [18–20]. As the price of glycerol is falling as fast as biodiesel plants are becoming popular, research is currently finding new outlets to convert glycerol into high-added value products that improve the economy of the whole process [21–23]. Glycerol etherification with *tert*-butyl alcohol (TBA) is an acid catalyzed reaction, resulting in a mixture of mono-*tert*-butylglycerol (MTBG), di-*tert*-butyl-glycerol (DTBG) and tri-*tert*-butylglycerol (TTBG), together with some unwanted by-products resulting of polymerization reactions. MTBG is the main product obtained in glycerol etherification, as a result of the electrophilic attack of the *tert*-butyl cation (a tertiary carbocation) preferably on the primary carbon of glycerol due to steric hindrance and electrostatic effects exerted by OH glycerol groups. However, DTBG and TTBG are excellent additives with a large potential for diesel and biodiesel reformulation [24–26] because of their ease of blending and non-polar properties. Thus, when DTBG and TTBG were incorporated in standard 30–40% aromatic-containing diesel fuel, emissions of particulate matter, hydrocarbons, carbon monoxide, and unregulated aldehydes decreased significantly [25,26].

The use of TBA as an etherification agent, in substitution of isobutylene (IB), avoids both the need for the use of solvents able to dissolve glycerol, such as dioxane or dimethyl sulfoxide, and the mass transfer limitation phenomena related to the complex three-phase system [26]. Although the water formed when using TBA as a reagent seems to have an inhibition effect on glycerol *tert*-butylation, decreasing the selectivity to DTBG and TTBG. Reactions are typically promoted between 353 and 393 K, with TBA:glycerol molar ratio of 4:1. The reaction is catalyzed by a highly acidic solid acid catalyst, which initiates the reaction between two alcohols [27]. Brønsted acid sites of sulfonic group containing catalyst have proven to be very effective in the reaction, and there are a great number of studies using sulfonated catalysts. Conversion values close to 100% are reached after 5–8 h of reaction, with selectivity to DTBG + TTBG as high as 80% using acidic resin catalysts (Amberlyst

type) [28]. Klepácová et al. [28] also tested zeolites H-Y and H-Beta but, on the whole, selectivity to DTBG + TTBG around 25% was achieved for this reaction, and TTBG was not detected when using these zeolites. This has been attributed to steric hindrance effects because of the microporosity of the zeolites [27]. Frusteri et al. used lab-made silica supported acid catalysts, but did not improve the catalytic results of Amberlyst [29]. Similarly, González et al. [30] evaluated zeolites H-Y and H-Beta with different treatments (dealumination, desilication etc) and also observed lower conversion and selectivity and selectivity to TTBG was not greater than 1%. When using isobutylene, González et al. [31] obtained 96% conversion and selectivity to DTBG + TTBG of 37%, of which 8% corresponded to TTBG when using fluorinated hierarchical Beta zeolite, indicating that the additional porosity in fact favors the selectivity to DTBG + TTBG.

In the present paper, we have investigated the effect of porosity of hierarchical MFI type zeolite prepared by using a multiammonium surfactant as the zeolite SDA in a seed-assisted methodology. The glycerol etherification with *tert*-butanol was performed as a model reaction.

## 2. Experimental

The reagents used in this work were used without any previous treatment, unless specified otherwise. Two samples of commercial ZSM-5, MH 8014 and MH 3024E, were provided by Zeolyst company. The samples present Si/Al ratio of 40 and 15, and were called Zeolyst-15 and Zeolyst-40 respectively. The polymer ion exchange Amberlyst 15 (Aldrich) was also used in this study. The synthesized catalysts were denoted as MFI-X-Y, where X denotes the morphology: unilamellar (UL), nanospunge (SD) or Bulk, and Y denotes the Si/Al molar ratio.

### 2.1. Synthesis of structure directing agent C<sub>22</sub>–6–6

The C<sub>22</sub>–6–6 surfactant of formula C<sub>22</sub>H<sub>45</sub>–N<sup>+</sup>(CH<sub>3</sub>)<sub>2</sub>–C<sub>6</sub>H<sub>12</sub>–N<sup>+</sup>(CH<sub>3</sub>)<sub>2</sub>–C<sub>6</sub>H<sub>13</sub> was prepared as described by Minkee et al. [32] and confirmed by <sup>1</sup>H NMR (Bruker Avance instrument 300 MHz) in CDCl<sub>3</sub>. The first nucleophilic substitution was typically performed using 16 g of 1-bromodocosane (TCI, 98%) and 70 g of *N,N,N',N'*-tetramethyl-1,6-diaminohexane (TCI, 98%), which were dissolved in acetonitrile and heated at 323 K under stirring for 48 h. The total substitution was confirmed by <sup>1</sup>H NMR, with the disappearance of the signal near 3.5 ppm. The solvent was evaporated and the product, denoted C<sub>22</sub>–6–0, was washed with ether and dried in a vacuum oven for 12 h. The product was redissolved in acetonitrile and two molar equivalents of 1-bromohexane added to the reaction for the second substitution. The mixture was held at 323 K under stirring until the disappearance of the signal near 2.3 ppm, indicating the formation of the second quaternary ammonium salt. The product was purified as described above.

### 2.2. Preparation of catalysts

#### 2.2.1. Unilamellar MFI nanosheets

Unilamellar type MFI zeolite was hydrothermally prepared using the C<sub>22</sub>–6–6 agent based com the procedure described by Park et al. [33]. The gel of molar composition 100 SiO<sub>2</sub>: x Al<sub>2</sub>O<sub>3</sub>: 39 Na<sub>2</sub>O: 7.5 C<sub>22</sub>–6–6: 4000 H<sub>2</sub>O, where x = 0.5 or 1.0, was obtained from sodium silicate (29% SiO<sub>2</sub>, 10.6% Na<sub>2</sub>O, Aldrich), sodium aluminate (53% Al<sub>2</sub>O<sub>3</sub>, 34% Na<sub>2</sub>O, Dae-Jung) and H<sub>2</sub>SO<sub>4</sub> (47%, Wako). In a polypropylene bottle, 1 g of surfactant and 4.1 g of sodium silicate were added to 7 mL of water, and remained under stirring until complete dissolution. Then 0.04 or 0.02 g of sodium aluminate were dissolved in 5 mL of water and this solution was added dropwise to

the previous mixture. Finally, the pH was adjusted to 12 with 2.3 M sulfuric acid. The mixture was aged for 12 h at 333 K under magnetic stirring, after which it was transferred to a stainless steel autoclave lined with Teflon, and a Teflon deflector inserted. The autoclave was placed into a rotating oven at 423 K and 150 rpm for at least 6 days, according to the Si/Al ratio. The precipitated product was washed with distilled water, dried and calcined at 853 K.

### 2.2.2. Nanosponge MFI type with addition of nucleating agent

The MFI nanosponge type was prepared with the C<sub>22–6–6</sub> directing agent and 5% weight of SiO<sub>2</sub>, regarding the amount in the synthesis gel, of zeolite ZSM-5 was added (in acid form with Si/Al ratio = 40, according to the methodology described by Jo et al. [14]). The gel molar composition of 100 SiO<sub>2</sub>: x Al<sub>2</sub>O<sub>3</sub>: 33 Na<sub>2</sub>O: 7.5 C<sub>22–6–6</sub>: 24 H<sub>2</sub>SO<sub>4</sub>: 5000 H<sub>2</sub>O was obtained from sodium silicate (29% SiO<sub>2</sub>, 10.6% Na<sub>2</sub>O, Aldrich), Al<sub>2</sub>(SO<sub>4</sub>)<sub>3</sub> (98%, Aldrich) and H<sub>2</sub>SO<sub>4</sub> (47%, Wako), where x = 0.5 or 1.0. In a polypropylene bottle, 1 g of surfactant was dissolved in 10 mL of water, and then an aqueous solution containing 0.13 or 0.07 g of aluminum sulphate was added slowly under stirring. The mixture was held at 333 K under stirring for 10 min. Then an aqueous solution containing 4.14 g of sodium silicate was slowly added to the polypropylene bottle. The mixture was aged for 3 h at 333 K under stirring. Then, the pH was adjusted to 12 with 4 mmol of H<sub>2</sub>SO<sub>4</sub>, and the gel aged for additional 3 h. Finally the nucleating agent Zeolyst-40 was added, and the gel was aged for 12 h. Later, it was transferred to a stainless steel autoclave lined with Teflon, and a Teflon baffle was inserted. The autoclave was placed in a rotating oven at 423 K for at least 3 days, according to the Si/Al ratio. The precipitated product was washed with distilled water, dried and calcined at 853 K.

### 2.2.3. MFI zeolite bulk

Conventional MFI zeolite was hydrothermally prepared using tetrapropylammonium bromide (98%, Aldrich). The gel of molar composition of 100 SiO<sub>2</sub>: x Al<sub>2</sub>O<sub>3</sub>: 33 Na<sub>2</sub>O: 7.5 C<sub>22–6–6</sub>: 4000 H<sub>2</sub>O, where x = 0.42, 0.71 or 1.25, was obtained from tetraethyl orthosilicate (98%, Aldrich), sodium aluminate (53% Al<sub>2</sub>O<sub>3</sub>, 34% Na<sub>2</sub>O, Dae-Jung) and NaOH (98%, Aldrich). In a polypropylene bottle, 0.4 g of NaOH, 0.028 g of sodium aluminate, 21 mL of water, and 0.5 g of tetrapropylammonium bromide were dissolved. The solution was stirred for 1 h. Then 4.1 g of tetraethyl orthosilicate was added at once and the solution was allowed to stir at 200 rpm for 6 h. Later, it was aged at 333 K for 2 days, when it was transferred to a stainless steel autoclave lined with Teflon. The autoclave was kept under static conditions at 453 K for 3 days. The precipitated product was washed with distilled water, dried and calcined at 853 K.

## 2.3. Characterization

X-ray powder diffraction (XRD) patterns for each sample were obtained using a Rigaku Multiflex diffractometer with Cu K $\alpha$  radiation ( $\lambda=0.1541\text{ nm}$ ), at 40 kV and 30 mA. Scanning electron microscopy (SEM) images were obtained with a FEI VERIOS operating at 1 kV without metal coating. Transmission electron microscopy (TEM) images were taken with a Philips F30 Tecnai at an accelerating voltage of 300 kV (Cs = 0.6 mm, point resolution 0.17 nm). Nitrogen adsorption-desorption isotherms were measured using an Micromeritics Tristar II volumetric adsorption analyzer at 77 K, with the samples being outgassed for 4 h at 573 K under vacuum prior to measurement. The Brunauer–Emmett–Teller (BET) equation was used to calculate the surface area from the adsorption branch of isotherm in the range of  $p/p_0$  between 0.1 and 0.3; meanwhile, the total pore volume was evaluated from the amount of adsorbed argon at  $p/p_0=0.95$ . The mesopore size distributions were then derived from the adsorption branch of the N<sub>2</sub> isotherms using the Barrett–Joyner–Halenda

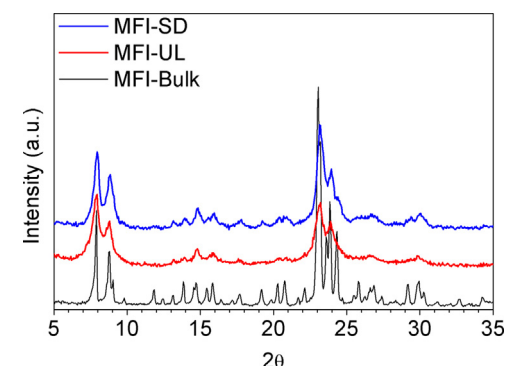


**Fig. 1.** Typical diffraction pattern for nanostructured and bulk MFI zeolites.

(BJH) algorithm. The atomic ratio of Si to Al in each zeolite sample was analyzed using an OP-TIMA 4300 DV (Perkin-Elmer) ICP/AES; 0.1 g of zeolite sample being first completely dissolved in 10 mL of HF/HNO<sub>3</sub>/H<sub>2</sub>O (v:v:v = 1:1:1), and then added to 40 mL of a saturated boric acid solution.

### 2.4. Catalytic tests

Catalytic tests were performed in Teflon-lined stainless steel autoclave, typically at 393 K, with 5 wt.% of catalyst and TBA:glycerol molar ratio of 4:1. The reaction time was considered after the system achieved operating temperature (around 10 min after closing the reactor). Samples were analyzed by gas chromatography (Agilent 7890A, FID, DB-Wax 30 m × 0.25 mm × 0.25 μm) using acetonitrile as the internal standard. The identification of the reaction products was done by GCMS (Shimadzu QP-2010Plus, SGE BP-20-strong Wax 30 m × 0.25 mm × 0.25 μm) and confirmed according to the method described by Jamroíz et al. [34].

Glycerol conversion (%), product yield (%), and product selectivity (%) were calculated using the following equations

$$\text{Glycerol Conversion (\%)} = \frac{\text{moles of reacted glycerol}}{\text{moles of taken glycerol}}$$

$$\text{Product Yield (\%)} = \frac{\text{moles of obtained product}}{\text{moles of taken glycerol}}$$

$$\text{Product Selectivity (\%)} = \frac{\text{moles of obtained product}}{\text{total moles of products}}$$

## 3. Results and discussion

### 3.1. Characterization of catalysts

The catalysts were prepared as described above and their structure confirmed by X-ray diffraction, Fig. 1. It is possible to note a greater number of signals in bulk zeolite than in nanostructured zeolites. While bulk zeolite crystals have dimensions in the micrometer range, and grow in all directions, nanostructured zeolites are extremely thin in at least one direction, causing the diffraction plans containing that direction to disappear.

Nitrogen physisorption analysis (Fig. 2) of hierarchical zeolites afforded Type IV isotherm according to the IUPAC classification, with type II hysteresis characteristic of materials with high mesoporosity. A high slope of the relative pressure suggests an increase in the homogeneity of the size of the mesopores, confirmed by the distribution of pores. There is considerable difference in the distribution of pores between unilamellar nanosheet and nanosponge type zeolite. In the first case, the nanosheets are arranged in a

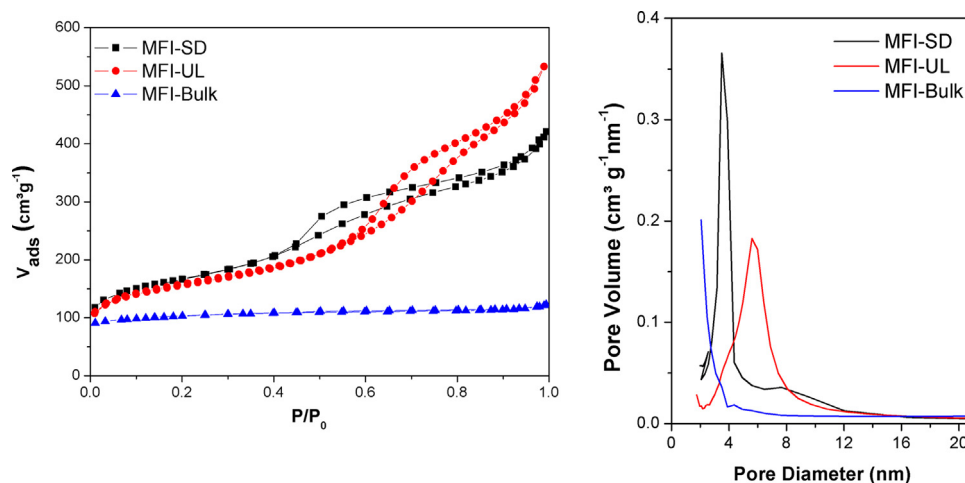


**Fig. 2.** Nitrogen adsorption/desorption isotherms, and pore volume distribution (BJH) of catalysts.

**Table 1**

Textural properties of catalysts.

| Sample      | $S_{\text{BET}}$ ( $\text{m}^2/\text{g}$ ) | $V_{\text{tot}}^{\text{a}}$ ( $\text{cm}^3/\text{g}$ ) | $V_{\text{micro}}^{\text{b}}$ ( $\text{cm}^3/\text{g}$ ) | $V_{\text{meso}}^{\text{c}}$ ( $\text{cm}^3/\text{g}$ ) | Mesopore size <sup>d</sup> (nm) |
|-------------|--|--|--|---|---------------------------------|
| MFI-UL-50   | 532  | 0.82   | 0.097  | 0.785   | 6.8                             |
| MFI-UL-100  | 575  | 0.79   | 0.095  | 0.695   | 6.4                             |
| MFI- SD-50  | 665  | 0.79   | 0.087  | 0.703   | 4.5                             |
| MFI-SD-100  | 583  | 0.61   | 0.095  | 0.515   | 4.9                             |
| MFI-bulk-20 | 359  | 0.18   | 0.098  | 0.082   | 2.4                             |
| MFI-bulk-50 | 367  | 0.17   | 0.105  | 0.065   | 2.3                             |

<sup>a</sup> Total volume at  $P/P_0 = 0.95$ .

<sup>b</sup> Values obtained from t-plot.

<sup>c</sup> Mesopore volume obtained from the difference between total volume and micropore volume.

<sup>d</sup> Mesopore size obtained by BJH method on the desorption isotherm.

more disordered manner, causing the pore size distribution to be broader. The nanospangle presents a more narrow distribution due to the formation of pillared structures, where individual nanosheets are arranged in a sponge-like morphology in which adjacent nanosheets support each other even after removal of the directing agent after calcination.

The textural properties shown in Table 1 are consistent with the ones reported by Jo et al. [14]. As expected, nanospangle zeolite properties are slightly lower than the nanosheet, but its pore distribution is narrower, as explained before.

MFI-UL-50 presented surface area of  $532 \text{ m}^2/\text{g}$ , total pore volume of  $0.82 \text{ cm}^3/\text{g}$  and pore diameter of  $6.8 \text{ nm}$ , while MFI-UL-100 showed slightly higher surface area ( $575 \text{ m}^2/\text{g}$ ), but lower total pore volume and pore diameter,  $0.79 \text{ cm}^3/\text{g}$  and  $5.8 \text{ nm}$ , respectively. In the case of nanospangles, an opposite effect is observed: MFI- SD-50 presented surface area of  $665 \text{ m}^2/\text{g}$ , total pore volume of  $0.79 \text{ cm}^3/\text{g}$  and pore diameter of  $4.5 \text{ nm}$ , while MFI-SD-100 showed lower surface area and total pore volume,  $583 \text{ m}^2/\text{g}$  and  $0.61 \text{ cm}^3/\text{g}$ , respectively but a higher pore diameter ( $4.9 \text{ nm}$ ).

The difference between hierarchical zeolites and conventional, as evidenced by the textural properties can be viewed through the scanning and transmission microscopy shown in Fig. 3. Unilamellar nanosheet presented flocculate morphology, and no particles of aluminum- amorphous silicate or bulk zeolite were found. Its transmission microscopy reveals that nanosheets grow preferentially in only two axes, whilst the third is formed by a few layers MFI. In the case of nanospangle MFI the pillared structures described above can be easily observed. In transmission microscopy, it can be assumed that nanospangle is similar to nanosheet zeolite, except for the greater number of MFI layers, typically of  $2.5 \text{ nm}$  thickness.

**Table 2**

Acid site concentration of catalysts.

| Sample      | Acid sites (mmol/g) <sup>a</sup> |
|-------------|----------------------------------|
| MFI-SD-50   | 0.37                             |
| MFI-SD-100  | 0.28                             |
| MFI-UL-50   | 0.73                             |
| MFI-UL-100  | 0.41                             |
| Zeolyst 15  | 0.83                             |
| Zeolyst 40  | 0.40                             |
| MFI-bulk-20 | 0.99                             |
| MFI-bulk-50 | 1.05                             |

<sup>a</sup> Obtained from the 2nd signal.

Corroborating the diffraction data, the bulk zeolite presents very well defined crystals, which grow in all axes, reaching up to  $1 \mu\text{m}$ .

The acidity of the solid was checked by thermal desorption of ammonia. This analysis presents a limitation in the case of nanostructured materials, since they generate more than one signal in the desorption curve Bulk MFI presents two signals, while nanostructured presents three. To calculate the concentration of acid sites (Table 2), the area corresponding to the second signal was used. The first signal is related to physisorption of ammonia, which can be removed after a prolonged degassing at  $373 \text{ K}$  for  $16 \text{ h}$  [35] and the third one is generated from dehydration of silanol groups, which is enhanced in nanostructured materials. Catalysts containing lower Si/Al ratios showed higher concentrations of acid sites, as expected, although for a particular ratio the concentration varied according to the morphology type nanospangle MFI zeolites showed much lower acidity than unilamellar nanosheets.

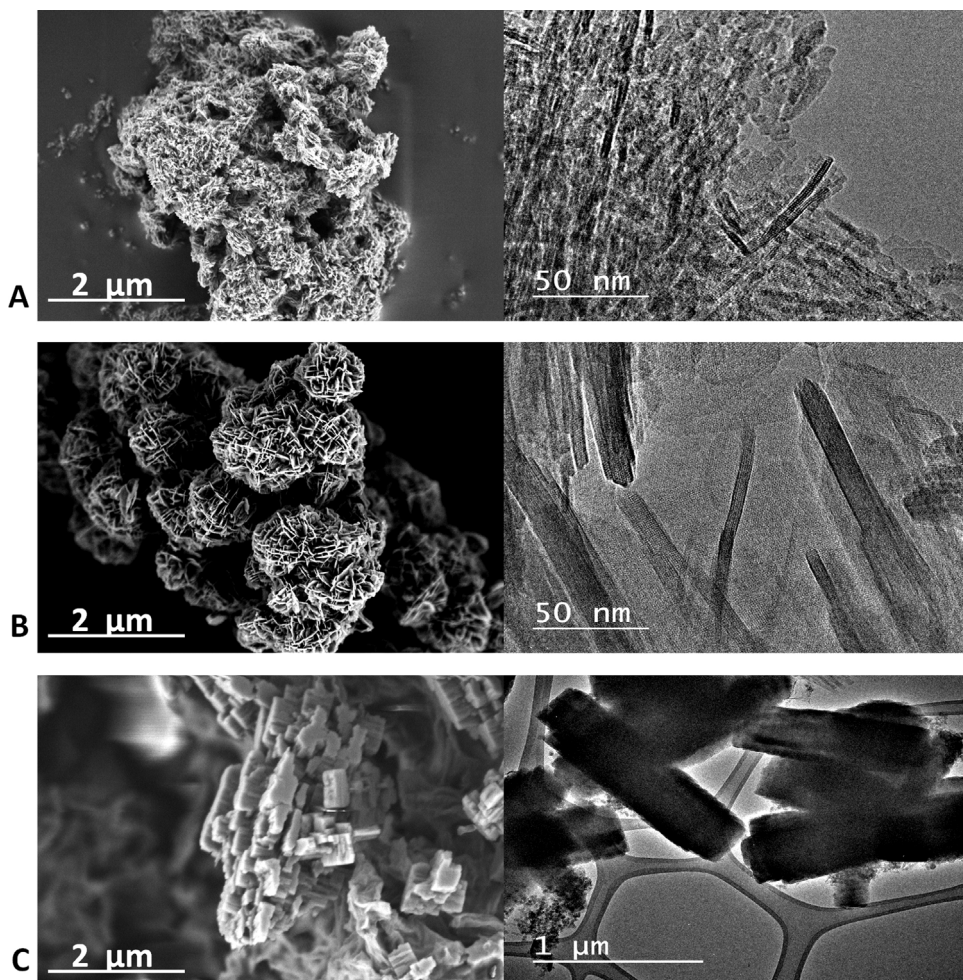
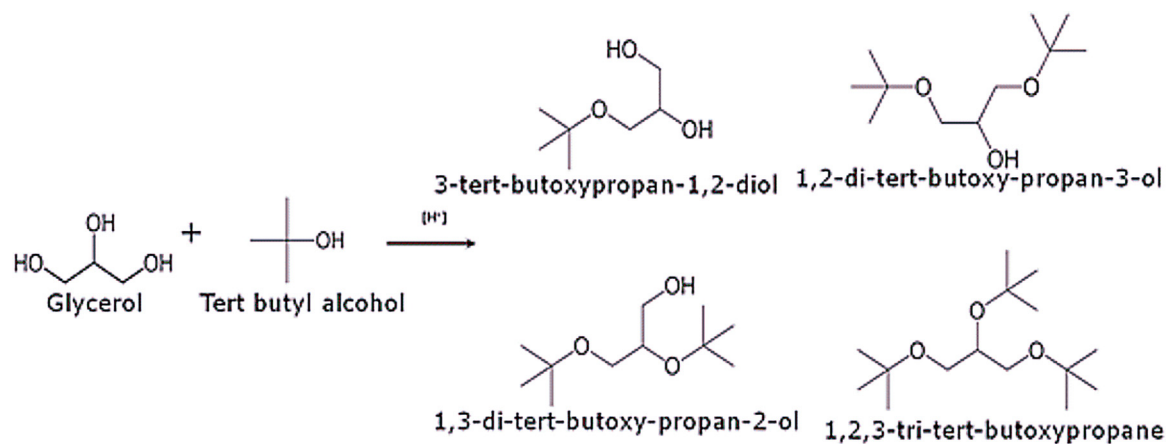


**Fig. 3.** Scanning electron micrographs (left) and transmission electron micrographs (right) of (A) unilamellar MFI nanosheet (B) MFI Nanospunge and (C) bulk MFI.



**Scheme 1.** Glycerol etherification with *tert*-butanol

### 3.2. Catalytic activity

Etherification of glycerol with *tert*-butanol was carried out with the prepared catalysts aiming at the production of higher ethers DTGB and TTBG, as presented in Scheme 1. The reaction conditions, such as reaction time, temperature and glycerol/TBA molar ratio, previously optimized by our research group [36–40] were used in this study and provided the best results indeed.

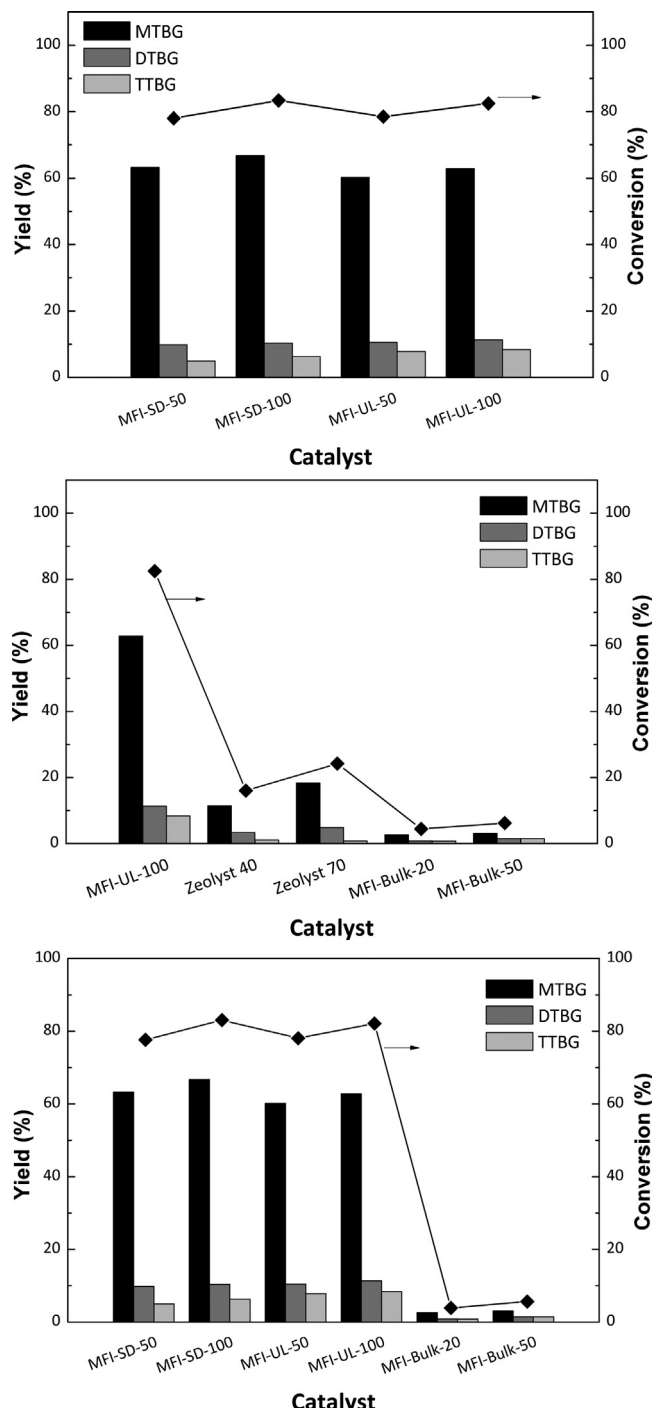
Both unilamellar nanosheets and nanospunge MFI zeolites were very active for the glycerol etherification with *tert*-butanol, generating conversions between 78 and 83% after 12 h of reaction, as shown in Fig. 4.

Selectivity to high ethers was similar, ranging from nearly 20% for nanosponge zeolites and 24% for unilamellar nanosponge, as shown in Table 3.

The catalysts processing a unilamellar nanosheet like morphology provided 10% selectivity to TTBG, while MFI nanospunge

**Table 3**Glycerol etherification with *tert*-butanol.

| Catalyst    | Conversion (%) | Selectivity to MTBG (%) | Selectivity to DTBG + TTBG (%)* |
|-------------|----------------|-------------------------|---------------------------------|
| MFI-SD-50   | 78.0           | 81.1                    | 18.7 (6.4)                      |
| MFI-SD-100  | 83.4           | 80.0                    | 20.0 (7.6)                      |
| MFI-UL-50   | 78.5           | 76.7                    | 23.3 (9.9)                      |
| MFI-UL-100  | 82.5           | 76.1                    | 23.9 (10.2)                     |
| Zeolyst 20  | 15.8           | 72.0                    | 28.0 (traces)                   |
| Zeolyst 50  | 24.1           | 76.1                    | 23.9 (traces)                   |
| MFI-bulk-20 | 4.3            | 61.3                    | 38.7 (traces)                   |
| MFI-bulk-50 | 6.0            | 50.8                    | 49.2 (traces)                   |

**Fig. 4.** Catalytic activity of solids in glycerol etherification with *tert*-butanol at 393 K for 12 h.

zeolites reached 7.6%. This result can be attributed to the larger pores of the nanosheet zeolite, which are able to better accommodate bulkier products. These values are comparable to the ones obtained by González et al. [31], using isobutylene and a fluorinated hierarchical beta zeolite as the catalyst, for 24 h. The authors reported a 96% conversion and selectivity to high ethers of 37%, of which 8% corresponded to TTBG.

Only in the case of nanostructured MFI zeolites, no further surface treatment was necessary and the reaction time was 12 h. Furthermore, the unique morphologies obtained by the described method of synthesis can play an important role on the catalytic activity, as hierarchical zeolites obtained by treatments such as dealumination and desilication of microporous H-Y, H-Beta and ZSM-5 pristines are reported to be inefficient for production of TTBG, with no selectivity or values lower than 1% [30].

Tested bulk materials yielded traces (less than 1%) of TTBG, in accordance to the literature. The commercial samples were more active than the prepared analogues, even though they presented lower concentrations of acid sites. Likewise, when comparing a single morphology type, materials containing more aluminum in the zeolite framework, thus higher amounts of acid sites, were less active. Once aluminum substitutes for silicon in a tetrahedral framework, a strong Brønsted acid is created only if there are no second-neighbor aluminum atoms. Thus, decreasing the Si/Al ratio in the zeolite framework increases the number of acid sites, but also increases the neighboring of aluminum atoms, in which case each Brønsted acid site becomes somewhat weaker as the population of protons increases due to proton crowding in the zeolite pores. On the other hand, if extra-framework aluminum is present, a Lewis acid site is created [41]. Since the increase in the number of acid sites did not respond accordingly to the catalytic activity, and being this reaction mainly catalyzed by Brønsted sites, this result is therefore related to the nature of the sites created: the generation of weaker Brønsted acid sites or the increase in Lewis acid sites.

#### 4. Conclusions

By altering the synthesis methodology of unilamellar MFI nanosheet zeolite it is possible to obtain a nanospunge-like morphology by using the same structure-directing agent. The commercial zeolite added to the gel synthesis acts as a nucleating agent, accelerating the crystallization process. These materials presented a thinner pore size distribution attributed to a more regular arrangement where individual nanosheets support each other, forming a pillared structure, preserved after calcination. Both nanospunge and nanosheet zeolites were far more active than the bulk samples yielding conversions up to 83%. Their hierarchical arrangement of pores also favored the production of higher ethers. Selectivity to TTBG as high as 10% was obtained with unilamellar MFI containing a Si/Al ratio of 100, a value first reported for untreated zeolites. The acid sites located on the external surfaces are accessible for the reaction of bulky reactants. The increase in the aluminum content of zeolites possibly weakened the strength of active acid sites, causing the catalytic activity to be slight lower.

## Acknowledgements

The authors acknowledge the financial support from FAPESP-Brazil (Project No. 2013/21160-6 e 2014/18529-0), CAPES-Brazil (Project No. 2083-13-2) and CNPq-Brazil (Project No. 441936/2014-8).

## References

- [1] J. Perez-Ramirez, C.H. Christensen, K. Egeblad, C.H. Christensen, J.C. Groen, *Chem. Soc. Rev.* 37 (2008) 2530–2542.
- [2] Y. Seo, K. Cho, Y. Jung, R. Ryoo, *ACS Catal.* 3 (2013) 713–720.
- [3] T. Tang, C. Yin, L. Wang, Y. Ji, F.-S. Xiao, *J. Catal.* 249 (2007) 111–115.
- [4] M.S. Holm, E. Taarning, K. Egeblad, C.H. Christensen, *Catal. Today* 168 (2011) 3–16.
- [5] K. Möller, T. Bein, *Chem. Soc. Rev.* 42 (2013) 3689–3707.
- [6] K. Na, M. Choi, R. Ryoo, *Microporous and Mesoporous Mater.* 166 (2013) 3–19.
- [7] J. Scherzer, *J. Catal.* 54 (1978) 285–288.
- [8] J. Lynch, F. Raatz, P. Dufresne, *Zeolites* 7 (1987) 333–340.
- [9] Y. Sasaki, T. Suzuki, Y. Takamura, A. Saji, H. Saka, *J. Catal.* 178 (1998) 94–100.
- [10] W.J. Roth, C.T. Kresge, J.C. Vartuli, M.E. Leonowicz, A.S. Fung, S.B. McCullen, MCM-36: The first pillared molecular sieve with zeolite properties, in: H.G.K.I.K. H.K. Beyer, J.B. Nagy (Eds.), *Studies in Surface Science and Catalysis*, Elsevier, 1995, pp. 301–308.
- [11] A. Corma, V. Fornes, S.B. Pergher, T.L.M. Maesen, J.G. Buglass, *Nature* 396 (1998) 353–356.
- [12] M. Choi, K. Na, J. Kim, Y. Sakamoto, O. Terasaki, R. Ryoo, *Nature* 461 (2009) 246–249.
- [13] K. Na, C. Jo, J. Kim, K. Cho, J. Jung, Y. Seo, R.J. Messinger, B.F. Chmelka, R. Ryoo, *Science* 333 (2011) 328–332.
- [14] C. Jo, K. Cho, J. Kim, R. Ryoo, *Chem. Commun.* 50 (2014) 4175–4177.
- [15] C.J.H. Jacobsen, C. Madsen, J. Houzvicka, I. Schmidt, A. Carlsson, *J. Am. Chem. Soc.* 122 (2000) 7116–7117.
- [16] M. Choi, H.S. Cho, R. Srivastava, C. Venkatesan, D.H. Choi, R. Ryoo, *Nat. Mater.* 5 (2006) 718–723.
- [17] M. Choi, R. Srivastava, R. Ryoo, *Chem. Commun.* (2006) 4380–4382.
- [18] R.G.O. D'Aquino, *Chem. Eng.* 114 (2007) 31–37.
- [19] M. Pagliaro, R. Ciriminna, H. Kimura, M. Rossi, C. Della Pina, *Angew. Chem. Int. Ed.* 46 (2007) 4434–4440.
- [20] J. Feng, M. Yuan, H. Chen, *Prog. Chem.* 19 (2007) 651–658.
- [21] M. Pagliaro, R. Ciriminna, H. Kimura, M. Rossi, C. Della Pina, *Eur. J. Lipid Sci. Technol.* 111 (2009) 788–799.
- [22] M. Pagliaro, R. Ciriminna, H. Kimura, M. Rossi, C. Della Pina, *Angew. Chem. Int. Ed.* 46 (2007) 4434–4440.
- [23] J. Barrault, F. Jerome, *Eur. J. Lipid Sci. Technol.* 110 (2008) 825–830.
- [24] T.S. Viinikainen, R.S. Karinen, A.O.I. Krause, Conversion of glycerol into traffic fuels, in: *Catalysis for Renewables*, Wiley-VCH Verlag GmbH & Co. KGaA, 2007, pp. 209–222.
- [25] H.S. Kesling, L.J. Karas, F.J. Liotta, in: *Google Patents*, 1994.
- [26] M. Marchionna, R. Patrini, D. Sanfilippo, A. Paggini, F. Giavazzi, L. Pellegrini, From natural gas to oxygenates for cleaner diesel fuels, in: J.J.S.E. Iglesia, T.H. Fleisch (Eds.), *Studies in Surface Science and Catalysis*, Elsevier, 2001, pp. 489–494.
- [27] K. Klepacova, D. Mravec, M. Bajus, *Appl. Catal. A: Gen.* 294 (2005) 141–147.
- [28] K. Klepacova, D. Mravec, A. Kaszonyi, M. Bajus, *Appl. Catal. A: Gen.* 328 (2007) 1–13.
- [29] F. Frusteri, F. Arena, G. Bonura, C. Cannilla, L. Spadaro, O. Di Blasi, *Appl. Catal. A: Gen.* 367 (2009) 77–83.
- [30] M.D. González, Y. Cesteros, P. Salagre, *Appl. Catal. A: Gen.* 450 (2013) 178–188.
- [31] M.D. González, P. Salagre, M. Linares, R. García, D. Serrano, Y. Cesteros, *Appl. Catal. A: Gen.* 473 (2014) 75–82.
- [32] C. Minkee, C. Hae Sung, S. Rajendra, V. Chithravel, C. Dae-Heung, R. Ryong, *Nat. Mater.* 5 (2006) 718–723.
- [33] W. Park, D. Yu, K. Na, K.E. Jelfs, B. Slater, Y. Sakamoto, R. Ryoo, *Chem. Mater.* 23 (2011) 5131–5137.
- [34] M.E. Jamróz, M. Jarosz, J. Witowska-Jarosz, E. Bednarek, W. Tęcza, M.H. Jamróz, J.C. Dobrowolski, J. Kijeński, *Spectrochim. Acta Part A: Mol. Biomol. Spectrosc.* 67 (2007) 980–988.
- [35] M. Niwa, N. Katada, *Catal. Surv. Asia* 1 (1997) 215–226.
- [36] M. Mantovani, E.M. Aguiar, W.A. Carvalho, D. Mandelli, M. Gonçalves, *Quím. Nova* 38 (2015) 526–532.
- [37] M. Gonçalves, V.C. Souza, T.S. Galhardo, M. Mantovani, F.C.A. Figueiredo, D. Mandelli, W.A. Carvalho, *Ind. Eng. Chem. Res.* 52 (2013) 2832–2839.
- [38] M. Gonçalves, M. Mantovani, W.A. Carvalho, R. Rodrigues, D. Mandelli, J. Silvestre Albero, *Chem. Eng. J.* 256 (2014) 468–474.
- [39] T.S. Galhardo, N. Simone, M. Gonçalves, F.C.A. Figueiredo, D. Mandelli, W.A. Carvalho, *ACS Sustainable Chem. Eng.* 1 (2013) 1381–1389.
- [40] P.A. Celdeira, M. Gonçalves, F.C.A. Figueiredo, S.M.D. Bosco, D. Mandelli, W.A. Carvalho, *Appl. Catal. A: Gen.* 478 (2014) 98–106.
- [41] P. Somasundaran, *Encyclopedia of Surface and Colloid Science*, second ed., eight-vol. Set (Print), Taylor & Francis, 2006.